PHYSICAL REVIEW B **79**, 201405(R) (2009)

Interactions between Fermi surfaces and Brillouin zone boundaries and phase stability of embedded metallic nanoparticles

Y. Nagai,[1,2] T. Toyama,[1] Z. Tang,[3,4] K. Inoue,[1] T. Chiba,[1] M. Hasegawa,[3,5] S. Hirosawa,[6] and T. Sato[6]
[1]*The Oarai Center, Institute for Materials Research, Tohoku University, Oarai, Ibaraki 311-1313, Japan*
[2]*Studiecentrum voor Kernenergie–Centre d'Etude de l'Energie Nucleaire (SCK-CEN), Boeretang 200, B-2400 Mol, Belgium*
[3]*Institute for Materials Research, Tohoku University, Sendai 980-8577, Japan*
[4]*Key Laboratory of Polar Materials and Devices (Ministry of Education of China), East China Normal University, Shanghai 200241, People's Republic of China*
[5]*Cyclotron and Radioisotope Center, Tohoku University, Sendai 980-8578, Japan*
[6]*Department of Metallurgy and Ceramics Science, Tokyo Institute of Technology, Meguro-ku, Tokyo 152-0033, Japan*
(Received 16 March 2009; published 22 May 2009)

A general approach is outlined to predict the chemical compositions of solute nanoclusters embedded in materials with nearly free electrons. Based on the experimental results of the two-dimensional angular correlation of positron annihilation radiation and the corresponding theoretical calculations, we show that the Fermi surface (FS)–Brillouin zone interaction is a key to understand the chemical composition realized in solute nanoclusters because the presence of FS necks at zone boundaries causes a reduction in electron energy due to the band-gap effect.

DOI: 10.1103/PhysRevB.79.201405 PACS number(s): 73.22.−f, 71.18.+y, 78.70.Bj

Solute nanoclusters in alloys play important roles in the electronic and magnetic properties of recent quantum devices and in the mechanical properties of structural materials. From a fundamental material physics point of view, it is of significant interest to reveal the formation mechanism and phase stability of the nanoclusters based on the understanding of their electronic structures.

In 2000, we reported that a positron, an antiparticle of an electron, is a self-seeking and site-selective probe of the solute nanoclusters.[1] It was confirmed that the positron can also be confined in solute nanoclusters with positron affinities higher than that of the matrix, even if the nanoclusters are free from open volume defects.[1–3] This unique characteristic of the positron enables us to obtain information regarding the electronic structure of the solute nanoclusters, which has not been studied using other techniques. By measuring the angular correlation distribution between the two annihilation gamma photons [angular correlation of annihilation radiation (ACAR) technique[4]], the electron momentum distribution in the nanoclusters can be directly obtained experimentally. The first example, the Fermi surface (FS) of bcc Cu nanoclusters coherently embedded in bcc Fe, has been clearly observed in Ref. 5 with use of the two-dimensional (2D) ACAR technique.[4,6] Through several observations of FS topologies of solute nanoclusters in other materials, we found a general rule to suggest the preferential chemical composition of solute nanoclusters coherent to a matrix with nearly free electrons. The purpose of this Rapid Communication is to explain the concept of the general rule using experimental 2D-ACAR results and corresponding theoretical calculations.

The concept was inspired from a classical discussion of FS–Brillouin zone (BZ) interaction (band-gap effects at BZ),[7,8] often expressed in terms of the so-called *Hume-Rothery* (HR) *rule*.[9,10] The concept of the HR rule is that if a free-electron model-type FS grows until it would contact a BZ boundary, it may be energetically favorable for the system to change the lattice structure to avoid the allocation of electronic states in the higher energy band so that the new BZ may still allocate k states in the lower energy band. According to this idea, a coherent and stable precipitate in a given matrix structure should choose its chemical compositions to have an optimized e/a ratio. In other words, when the lattice structure of the very early stage precipitates is fixed due to the coherency to the matrix, the chemical composition of the precipitates might be selected so that the FS-BZ interaction effectively acts to reduce the total electron band energy.

The material systems employed in this work are spherical Ag and Zn nanoclusters coherent to Al matrix. These systems are obtained as so-called Guinier-Preston (GP)-zones formed in Al-Ag and Al-Zn alloys. Al-2.0 at. % Ag and Al-3.0 at. % Zn single crystals were heated at 530 °C for 30 min and then quenched into iced water, followed by thermal aging at 140 °C for 15 s. In the phase diagram of Al-Ag there is an hcp (ζ) intermediate phase, while in that of Al-Zn there is no intermediate phase; Al and Zn are mutually immiscible at low temperature.[11] Thus, it is well known that the Ag-rich nanoclusters consists of a mixture of Ag and host Al atoms, while the Zn nanoclusters are nearly pure Zn in the aged states.[12,13] Positrons can be trapped due to the difference in affinity between solute vacancy-free nanoclusters and Al matrix if the cluster size is larger than the critical radius.[2] The number density of the clusters formed by the thermal aging is sufficiently high to trap all positrons before annihilation.[4] We have already identified positron trapping in the Ag-rich and nearly pure Zn nanoclusters using the coincidence Doppler broadening (CDB) method.[14] (The CDB method can measure the momentum distribution of elementally specific inner orbital electrons and thus enables chemical identification of the positron annihilation sites.[15,16])

2D-ACAR spectra were obtained using the machine of Anger camera type.[17] Spectra corresponding to the (100)-

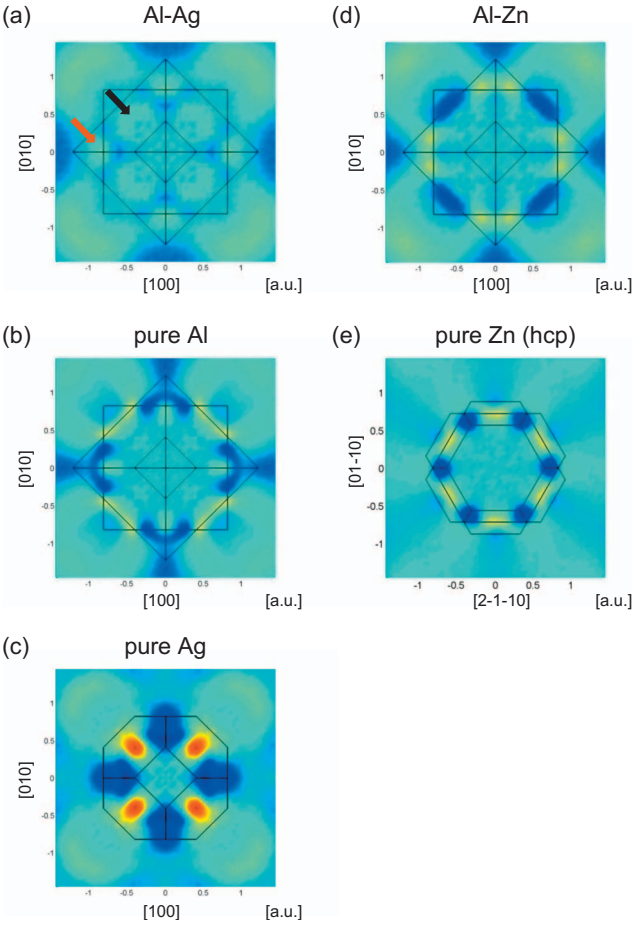

FIG. 1. (Color) Three-dimensional (3D) plots of experimental 2D-ACAR anisotropies projected along the [100] direction for (a) Al-2.0 at. % Ag (Ag-rich nanocluster), (b) pure Al, (c) pure Ag, (d) Al-3.0 at. % Zn (Zn nanocluster), and (e) pure Zn. (1) The color scale is determined so that dark red and dark blue are assigned to the top of the peaks and the bottom of the valleys, respectively. The peaks marked by red and black arrows in (a) arise from the *X*-point neck and the overlap of two *L*-point necks marked in Fig. 2, respectively.

plane projections of the momentum distribution of electron-positron pairs were measured. Approximately 5×10^7 counts of positron annihilations were accumulated for each spectrum. In addition to the Al-Ag and Al-Zn alloy samples, 2D-ACAR spectra were also measured for pure Al, Ag, and Zn single crystals as references. The 2D-ACAR spectra were normalized to the same total counts and smoothed to obtain a final isotropic momentum resolution of approximately 0.15 a.u. at the full width at half maximum (FWHM), and the anisotropies of the spectra were then obtained ($10^{-3}mc$ =0.137 a.u., where c is the speed of light and m is the electron rest mass). The anisotropy, which is defined as the differences between an observed 2D-ACAR and its cylindrical average, highlights the feature of the FS shape.[5]

The anisotropies of the 2D-ACAR spectra for the Al-Ag (Ag nanoclusters) and Al-Zn (Zn nanoclusters) alloys are shown in Figs. 1(a) and 1(d), respectively, together with those of pure Al, Ag, and Zn in Figs. 1(b), 1(c), and 1(e) as references. The anisotropies are fourfold symmetrized. The color scale is determined so that dark red and dark blue are assigned to the top of the peaks and the bottom of the valleys, respectively. The anisotropy characteristics of the Ag-rich nanoclusters are different from that of bulk Al due to positron trapping at the Ag-rich nanoclusters. The anisotropy is also different from that of bulk Ag, which indicates that the Ag-rich nanoclusters are not pure Ag but alloys of Ag and Al, resulting in different FS shapes. The anisotropy for Zn nanoclusters is different from that for bulk Zn; the crystal structure of Zn nanoclusters is the coherent fcc structure, not the hcp structure of bulk Zn.

In order to reveal the relationship between these features of the 2D-ACAR anisotropies and the FS topologies, the first-principles calculations of the electron band structures and the 2D-ACAR momentum distribution were performed for pure Al, Al_3Ag ($L1_2$ structure) AlAg ($L1_0$ structure), $AlAg_3$ ($L1_2$ structure), pure Ag, and pure Zn (fcc), using the full-potential linearized augmented plane wave (FLAPW) method implemented within the frame of two-component density functional (TCDF) theory.[18,19] The details of the present calculation method are described in Refs. 5 and 20, and references therein. By projecting the 3D electron-positron momentum densities along the [100] axes of the crystal structure, the 2D-ACAR distributions and their anisotropies are obtained, and the results are shown in Fig. 2. (In the theoretical anisotropy, the momentum resolution in the experiments is not taken into account, i.e., not smoothed.) The FSs are expressed in the *extended zone* scheme. It should be noted that the Ag-rich nanoclusters are considered to have disordered Ag-Al mixed structures rather than ordered Ag-Al compound structures. However, in the present calculations, we employed the several ordered structures because the calculations for disordered systems were not easy. Thus, the fine structures of the FSs of Al_3Ag ($L1_2$), AlAg ($L1_0$), and $AlAg_3$ ($L1_2$) would be blurred in the present case of the nanoclusters due to the effects of the disordered state and the finite size as stated below.

The experimental 2D-ACAR anisotropy for Ag-rich nanoclusters [Fig. 1(a)] is well reproduced by the calculated anisotropy for $AlAg_3$ and is different from those for the other Al-Ag systems (AlAg and Al_3Ag); both the experimental and calculated results for $AlAg_3$ show four narrower peaks at the momenta corresponding to the projection of the *X* point for fcc BZ (red arrow in Figs. 1 and 2) and four broader peaks at the momenta corresponding to the projection of the *L* point (black arrow in Figs. 1 and 2). By comparing the anisotropies and the FS of $AlAg_3$, the former corresponds to the six smaller FS necks at the *X* point and the latter corresponds to the eight larger FS necks at the *L* point. It should be noted that the experimental anisotropy has slightly weaker amplitude than the calculated anisotropy, which is considered to be due to the size effect of the clusters, i.e., the *smearing* of the momentum distribution,[21,22] as well as substitutionally disordered phase effects.

The experimental 2D-ACAR anisotropy for Zn nanoclusters [Fig. 1(d)] is very similar to the calculated anisotropy for pure Zn (fcc) as expected because the Zn nanoclusters are nearly pure Zn coherent to the Al (fcc) matrix. Both the experimental and calculated results show four peaks at the momenta corresponding to the projection of the *X* point for

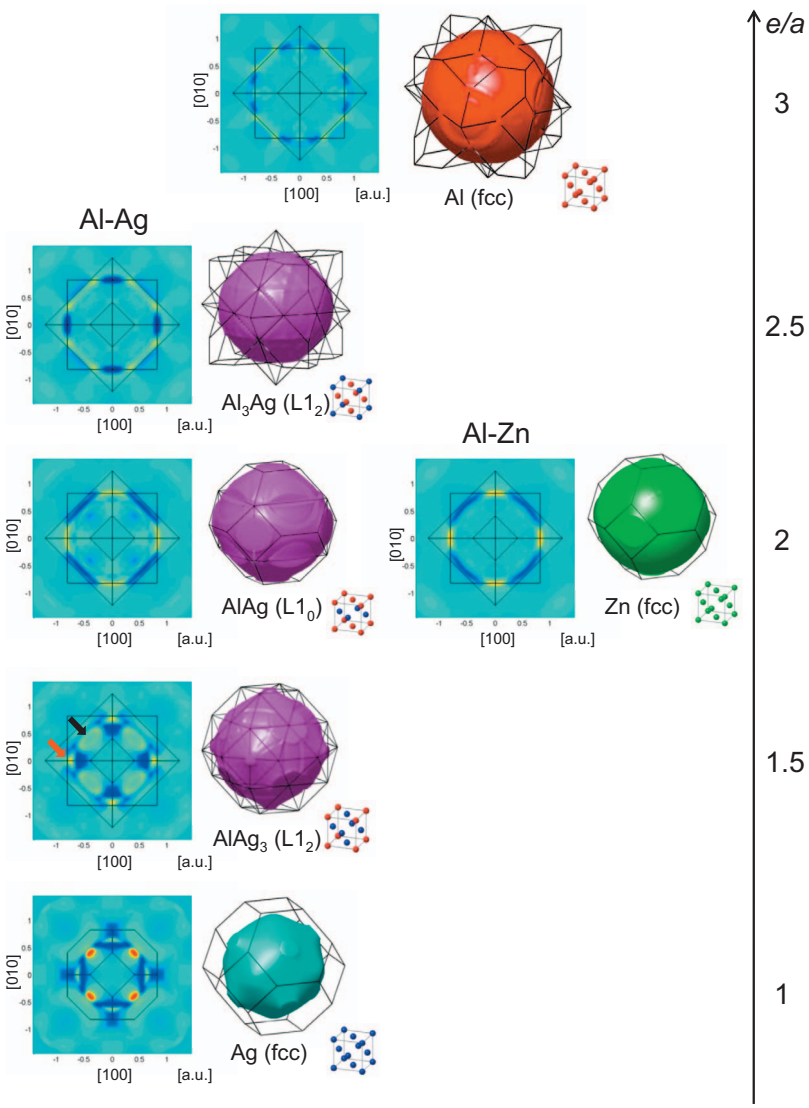

FIG. 2. (Color) 3D plots of calculated 2D-ACAR anisotropies projected along the [100] direction and FSs by FLAPW calculations for pure Al, Al_3Ag ($L1_2$), AlAg ($L1_0$), $AlAg_3$ ($L1_2$), pure Ag, and pure Zn (fcc).

fcc BZ and corresponding to the six FS necks at the X point.

The chemical compositions for the Ag-rich nanoclusters (around 3/4) and the Zn nanoclusters (nearly pure Zn) are explained in terms of the FS-BZ interactions. Simply and generally, the presence of FS necks causes a reduction in the total electron energy due to the band-gap effect at the BZ. As shown in Fig. 2, the average electrons per atom (e/a) is a function of the Ag composition: $e/a=1$ for pure Ag, 1.5 for $AlAg_3$, 2 for AlAg, 2.5 for Al_3Ag, and 3 for pure Al. In the case of $e/a=1$, the FS has eight small necks at the L point, which is typical of monovalent fcc metals. With an increase in e/a, the radius of the FS increases within the framework of the free-electron scheme so that the necks at the L point become larger, and six necks at the X point are also formed for $e/a=1.5$, which should contribute to a reduction in the total electron band energy. The realistic band-structure calculation predicts the formation of necks as shown in Fig. 2, which is consistent with the HR rule. According to the HR rule, when the FS grows until it would contact the BZ boundary, a gap will form to persevere the electrons so that they will occupy the lower energy bands and the total band energy of the valence electrons will be reduced. However, the necks at the L point disappear because some of the electrons occupy the second BZ for $e/a=2$, and the necks at the X point also disappear for $e/a=2.5$. These features suggest that the increase in electrons per atom larger than ~ 2 is not preferable for reduction in the total electron band energy. Thus, it is reasonable that the Ag-rich nanoclusters in the aged state have a chemical composition that is almost $AlAg_3$.

In the case of the Zn nanoclusters, the FS topology is very similar to that of AlAg because both have $e/a=2$. The Zn nanoclusters exhibit no neck at the L point but large necks at the X point. If Al is mixed with the Zn nanoclusters, then e/a increases and the radius of the FS also increases, resulting in the disappearance of the X-point necks similar to the FS of Al_3Ag, which does not cause a reduction in the total electron energy.

Finally, it should be mentioned that this concept is very simplified and the materials employed may be ideal systems. A simple application of this approach finds exceptions, such as GP zones in the Al-Cu system, where the GP zone is layer-type Al_2Cu. For further discussion, several important effects should be taken into account. One is the effect of strain energy, although the strain energy in the present case is

small because the atomic sizes of Ag (0.144 nm) and Zn (0.133 nm) are very similar to that of Al (0.143 nm). Another is the effect of entropy; the chemical composition of the nanoclusters depends on the temperature at which they are formed because it is not internal energy but free energy that should be minimized. In addition, as future work, it would also be interesting to examine the dependence of the cluster size on the momentum distribution.

In summary, a general rule was proposed to suggest preferential chemical composition of solute nanoclusters coherent to matrix with nearly free electrons, based on 2D-ACAR experimental results for Ag-rich and Zn nanoclusters in Al and the corresponding theoretical calculations. The FS-BZ interaction is a key to understand the chemical composition realized in the solute nanoclusters because the presence of necks on the FS contributes to the reduction in the electron energy due to the band-gap effect.

This work was partially supported by a Grant-in-Aid for Scientific Research from the Ministry of Education, Culture, Sports, Science and Technology (MEXT) (Grants No. 17002009 and No. 18686077) and Toray Science Foundation. We thank Y. Kawazoe and the Information Science Group of Institute for Materials Research, Tohoku University for their continuous support for using the supercomputing resources.

[1] Y. Nagai, M. Hasegawa, Z. Tang, A. Hempel, K. Yubuta, T. Shimamura, Y. Kawazoe, A. Kawai, and F. Kano, Phys. Rev. B **61**, 6574 (2000).

[2] M. J. Puska and R. M. Nieminen, Rev. Mod. Phys. **66**, 841 (1994).

[3] G. Dlubek, Mater. Sci. Forum, **13-14**, 11 (1987); *Positron Annihilation*, edited by L. Dorikens-Vanpraet, M. Dorikens, and D. Segers (World Scientific, Singapore, 1989), p. 76, and references therein.

[4] R. N. West, in *Positron Spectroscopy of Solids*, edited by B. A. Dupasquier and A. P. Mills, Jr. (IOS, Amsterdam, 1995), p. 75.

[5] Y. Nagai, T. Chiba, Z. Tang, T. Akahane, T. Kanai, M. Hasegawa, M. Takenaka, and E. Kuramoto, Phys. Rev. Lett. **87**, 176402 (2001).

[6] K. Fujiwara and O. Sueoka, J. Phys. Soc. Jpn. **21**, 1947 (1966).

[7] *Physical Metallurgy*, edited by R. W. Cahn and P. Hassen (North-Holland, Amsterdam, 1996).

[8] U. Mizutani, *Introduction to the Electron Theory of Metals* (Cambridge University Press, Cambridge, 1995).

[9] W. Hume-Rothery, R. E. Smallman, and C. W. Hawoeth, in *The Structure of Metals and Alloys* (Maney, London, 1988).

[10] T. B. Massalski and U. Mizutani, Prog. Mater. Sci. **22**, 151 (1978).

[11] H. Okamoto, *Desk Handbook: Phase Diagrams for Binary Alloys* (ASTM International, Materials Park, Ohio, 2000).

[12] F. Ernst and P. Haasen, Phys. Status Solidi A **104**, 403 (1987).

[13] R. Ramlau and H. Löffler, Phys. Status Solidi A **68**, 531 (1981).

[14] Y. Nagai, Z. Tang, H. Ohkubo, K. Takadate, and M. Hasegawa, Radiat. Phys. Chem. **68**, 381 (2003).

[15] K. G. Lynn, J. R. MacDonald, R. A. Boie, L. C. Feldman, J. D. Gabbe, M. F. Robbins, E. Bonderup, and J. Golovchenko, Phys. Rev. Lett. **38**, 241 (1977).

[16] P. Asoka-Kumar, M. Alatalo, V. J. Ghosh, A. C. Kruseman, B. Nielsen, and K. G. Lynn, Phys. Rev. Lett. **77**, 2097 (1996).

[17] T. Chiba, T. Toyama, Y. Nagai, and M. Hasegawa, Phys. Status Solidi C **4**, 3993 (2007).

[18] E. Boronski and R. M. Nieminen, Phys. Rev. B **34**, 3820 (1986).

[19] M. J. Puska, A. P. Seitsonen, and R. M. Nieminen, Phys. Rev. B **52**, 10947 (1995).

[20] Z. Tang, M. Hasegawa, Y. Nagai, M. Saito, and Y. Kawazoe, Phys. Rev. B **65**, 045108 (2002).

[21] Z. Tang, T. Toyama, Y. Nagai, K. Inoue, Z. Q. Zhu, and M. Hasegawa, J. Phys.: Condens. Matter **20**, 445203 (2008).

[22] M. H. Weber, K. G. Lynn, B. Barbiellini, P. A. Sterne, and A. B. Denison, Phys. Rev. B **66**, 041305(R) (2002).